Astron. Astrophys. 359, 531–538 (2000)

ASTRONOMY AND ASTROPHYSICS

Magnetic field escape from a stellar convection zone and the dynamo-cycle period

L.L. Kitchatinov[1,2], **M.V. Mazur**[2], **and M. Jardine**[1]

[1] School of Physics and Astronomy, University of St Andrews, St Andrews, Fife, KY16 9SS, Scotland (lk9,mmj@st-andrews.ac.uk)
[2] Institute for Solar-Terrestrial Physics, P.O. Box 4026, Irkutsk, 664033, Russia (kit@iszf.irk.ru)

Received 20 October 1999 / Accepted 14 April 2000

Abstract. Traditionally, dynamo theories have predicted periods for stellar activity cycles that are much shorter than is observed. We argue that this problem can be solved by allowing for the non-free escape of magnetic fields through the surface boundary. New boundary conditions are suggested that largely reduce magnetic flux escape from the dynamo region compared to the traditional vacuum conditions. The effect of the new conditions is checked with a solar-type dynamo model in a spherical shell. The dynamo incorporates the helioseismologically-detected rotation law and prescribes all the key parameters in accord with the convection zone structure models. The cycle period increases by an order of magnitude and the critical dynamo number decreases in about the same proportion when the new boundary conditions are implemented. The observed 22-year period of the solar cycle can be reproduced. Also the ratio of toroidal-to-poloidal magnetic field is brought closer to observations in this way. Based on our dynamo model, an interpretation can be offered for the empirical relation between activity cycle period and rotation rate of the slowly rotating solar-type stars.

Key words: stars: magnetic fields – Sun: magnetic fields – turbulence

1. Introduction

Theoretical periods of activity cycles that are too short have remained for decades an unsolved problem of dynamo theory of stellar activity (Rüdiger 1994). Dynamo models produce oscillation periods of order of one year while the sun and other cool stars show roughly ten-times longer activity cycles (Baliunas et al. 1995).

Such long cycles are very surprising in view of plain estimations. The hydromagnetic dynamo is essentially the instability of conducting fluids to a seed magnetic field (cf., e.g., Krause & Rädler 1980). Therefore, the general condition for overstability that the regeneration time (oscillation period) of unstable disturbances should be shorter than the characteristic time of the acting dissipative processes (Chandrasekhar 1961) should be satisfied. Dissipation in stellar dynamos is mainly provided by turbulent diffusion. Hence, the diffusive time for the smallest available scale estimates the maximum oscillation period. The solar values for the convection zone depth, $d \simeq 200$ Mm, and the eddy diffusivity, $\eta_{\rm T} \simeq 10^{13}$ cm^2 s^{-1}, lead to the diffusion time, $T_{\rm d} = d^2/\eta_{\rm T} \simeq 1$ yr. Thus, it is no surprise that dynamo models show activity cycles of about the same duration. The observed period, $P_{\rm cyc} = 22$ yr, may, however, result from unrealistically deep convection zones or artificially low eddy diffusivity, and examples of both types can be found in the literature. Deep convection zones conflict, however, with the helioseismology data (Kosovichev et al. 1997) and stellar structure theory (Kippenhahn & Weigert 1994). The low- diffusivity assumption is internally contradictional because the solar outer layers are unstable to thermal convection with the diffusivities of order 10^{12} cm^2 s^{-1} (Tuominen et al. 1994). The latter argument would not apply if the eddy magnetic diffusivity were much smaller than the eddy viscosity and thermal conductivity. There are no indications, however, for the very large magnetic Prandtl number (Rüdiger 1989).

All the above arguments concern the distributed type of dynamos. The case with overshoot dynamos is even more problematic, however, because the time of mixing across the overshoot layer is even shorter (Stix 1995). This paper deals with distributed dynamos. Though the choice between the interface and distributed dynamo regimes is not the subject with the present paper, it may be noted that estimations of magnetic buoyancy for convecting fluids (Nordlund et al. 1992; Kitchatinov & Pipin 1993), Doppler–Zeeman imaging of stellar magnetic structure (Donaty & Cameron 1997; Donati 1999), and the probable detection of an activity cycle on a fully-convective star (Alekseev & Gerschberg 1998) all favour distributed dynamos.

Another problem, though related to that mentioned above, is that the value of the dynamo number,

$$\mathcal{D} = \frac{\alpha\Omega R^3}{\eta_{\rm T}^2}, \qquad (1)$$

needed for stellar-type dynamos to operate is too high. In this equation, Ω is the angular velocity, R is the stellar radius, and α is the alpha-parameter by cyclonic convection (Parker 1979). A representative threshold value for a dynamo in a spherical shell is $\mathcal{D} \gtrsim 10^4$ (cf. Krause & Rädler 1980). This means that it should be $\alpha \gtrsim 10$ m s^{-1} for a dynamo to operate in the solar

Send offprint requests to: L.L. Kitchatinov

convection zone. This value is too large. In particular, it leads to a ratio of poloidal-to-toroidal field amplitude,

$$\frac{B_{\rm p}}{B_{\rm t}} \simeq \left(\frac{\alpha}{\Omega R}\right)^{1/2} \gtrsim 0.1, \qquad (2)$$

while it is $B_{\rm p}/B_{\rm t} \lesssim 0.01$ according to observations. The value of α required is so large because the dissipation is too strong. Recalling that dynamo-cycle frequency increases with dynamo number returns us to the original problem of an oscillation period that is too short.

The above estimation of the decay time by vertical diffusion applies, however, only if generated magnetic flux escapes freely through the top boundary. The present paper exploits the idea that free escape may not be the real case. If the surface were a reflecting boundary instead, the horizontal rather than vertical scale would define the decay time increasing the oscillation period by a missing factor of about ten. The point that conditions for magnetic fields on a stellar surface may indeed be much closer to reflection than to free escape was first noted by Parker (1984). The physical reason for this is that the vertical convective motions should vanish on the surface so that the magnetic field frozen into the stellar matter can erupt through the photosphere only due to the nonlinear effect of the loop-formation instability. Parker (1984) estimated the fraction of escaping magnetic flux to the total flux generated over the solar cycle to be only 3%. The concept of restricted escape is further supported by recent Doppler-Zeeman imagines of stellar surfaces (Donati & Cameron 1997; Donati 1999; Donati et al. 1999) showing unipolar longitudinal belts of azimuthal magnetic fields. The unipolar belts cannot be compatible with open boundary conditions.

We formulate below the boundary conditions which largely reduce the magnetic flux loss from the dynamo region. The application of the new conditions to a solar-type dynamo model increases the cycle period. Also the poloidal-to-toroidal field ratio is brought closer to observations on this way.

2. The model

2.1. Basic equations and the model design

We simulate dynamo action in a solar-type convection zone by solving the mean-field induction equation,

$$\partial \boldsymbol{B}/\partial t \;=\; {\rm rot}\,(\boldsymbol{V}\times\boldsymbol{B} \;+\; \boldsymbol{\mathcal{E}})\,, \qquad (3)$$

in an outer spherical layer of thickness $0.3R$. The large-scale velocity field, $\boldsymbol{V}$, stands for a non-uniform rotation,

$$\boldsymbol{V} = \boldsymbol{e}_\phi r\,\sin\theta\,\Omega(r,\theta), \qquad (4)$$

where $\boldsymbol{e}_\phi$ is the azimuthal unit vector and $r,\ \theta$ and ϕ are the usual spherical coordinates. The angular velocity, Ω, is represented as the series expansion,

$$\Omega(r,\theta) \;=\; \Omega_0 \sum_{n=1}^{3}\sum_{m=0}^{4} \omega_{nm} \left(\frac{r}{R_\odot}\right)^m \frac{\bar{P}^1_{2n-1}(\cos\theta)}{\sin\theta}, \qquad (5)$$

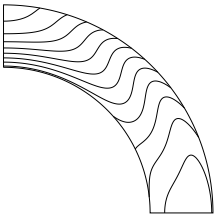

Fig. 1. Angular velocity isolines for differential rotation of the present model

Table 1. Coefficients of the expansion (5) for the solar internal rotation by SOHO-MDI data

n	ω_{n0}	ω_{n1}	ω_{n2}	ω_{n3}	ω_{n4}
1	-17.2006	92.1941	-173.0598	143.7571	-44.5361
2	3.75016	-13.21002	15.83814	-7.22336	0.77965
3	0.46158	-4.06427	10.87092	-11.56884	4.29199

where $\bar{P}^1_n$ are the normalized Legendre polynomials. Table 1 gives the values for the coefficients of the expansion (5) to reproduce closely the internal solar rotation (Belvedere et al. 2000) in accord with the helioseismology inversions of SOHO–MDI data (Kosovichev et al. 1997). The correspondent rotation law is shown in Fig. 1.

The mean electromotive force, $\boldsymbol{\mathcal{E}}$, of the induction equation (3) is due to the correlated fluctuations of magnetic, $\boldsymbol{B}'$, and velocity, $\boldsymbol{u}'$, fields,

$$\boldsymbol{\mathcal{E}} \;=\; \overline{\boldsymbol{u}'\times\boldsymbol{B}'} \;=\; \boldsymbol{\mathcal{E}}_{\rm diff} + \boldsymbol{\mathcal{E}}_{\rm gen} + \boldsymbol{\mathcal{E}}_{\rm pump}. \qquad (6)$$

This equation represents the electromotive force as a superposition of the contributions made by turbulent diffusion, magnetic field generation by the α-effect, and turbulent pumping.

The diffusive part allows for the rotationally-induced anisotropy and quenching (Kitchatinov et al. 1994),

$$\boldsymbol{\mathcal{E}}_{\rm diff} = -\eta\,{\rm rot}\boldsymbol{B} \;-\; \eta_{_\parallel}\boldsymbol{e}\times((\boldsymbol{e}\cdot\nabla)\boldsymbol{B})\,, \qquad (7)$$

where $\boldsymbol{e}=\boldsymbol{\Omega}/\Omega$ is the unit vector along the rotation axis and $\eta_{_\parallel}$ is the diffusivity excess along this axis compared to the transverse direction. The rotational effects on the diffusivities,

$$\eta \;=\; \eta_{\rm T}\phi(\Omega^*),\ \ \eta_{_\parallel} \;=\; \eta_{\rm T}\phi_{_\parallel}(\Omega^*), \qquad (8)$$

are quantified by the quenching functions,

$$\phi(\Omega^*) \;=\; \frac{3}{4\Omega^{*2}}\left(1 \;+\; \frac{\Omega^{*2}-1}{\Omega^*}{\rm tan}^{-1}\,(\Omega^*)\right),$$
$$\phi_{_\parallel}(\Omega^*) \;=\; \frac{3}{4\Omega^{*2}}\left(-3 \;+\; \frac{\Omega^{*2}+3}{\Omega^*}{\rm tan}^{-1}\,(\Omega^*)\right), \qquad (9)$$

of the local Coriolis number (normalized Coriolis frequency),

$$\Omega^* \;=\; 2\tau\Omega, \qquad (10)$$

where τ is the convective turnover time.

The generation part, $\boldsymbol{\mathcal{E}}_{\rm gen}$, of the mean electromotive force (6) is expressed in terms of the $\boldsymbol{\alpha}$-tensor,

$$\boldsymbol{\mathcal{E}}_{\rm gen} \;=\; \boldsymbol{\alpha}\circ\boldsymbol{B}. \qquad (11)$$

A mixing-length representation for this tensor for a density-stratified rotating fluid (Rüdiger & Kitchatinov 1993),

$$\begin{aligned}\alpha_{ij} &= -\hat{\alpha}\,(\boldsymbol{e}\cdot\boldsymbol{G})\,(\delta_{ij}a_1 + e_ie_ja_4)\\ &\quad -\hat{\alpha}\,(e_iG_j + e_jG_i)\,a_2,\end{aligned} \tag{12}$$

is applied. In this equation, $\boldsymbol{G}=\nabla\ln(\rho)$ is the density stratification vector and a_n-coefficients,

$$a_n = \eta_{\rm T}\mathcal{A}_n(\Omega^*), \tag{13}$$

are expressed in terms of the eddy diffusivity and new quenching functions,

$$\begin{aligned}\mathcal{A}_1(\Omega^*) &= \frac{3}{2{\Omega^*}^3}\left({\Omega^*}^2+6\right.\\ &\quad -\left.\frac{6+3{\Omega^*}^2-{\Omega^*}^4}{\Omega^*}\tan^{-1}(\Omega^*)\right),\\ \mathcal{A}_4(\Omega^*) &= \frac{3}{2{\Omega^*}^3}\left({\Omega^*}^2-30-\frac{2{\Omega^*}^4}{1+{\Omega^*}^2}\right.\\ &\quad +\left.\frac{30+9{\Omega^*}^2-{\Omega^*}^4}{\Omega^*}\tan^{-1}(\Omega^*)\right),\\ \mathcal{A}_2(\Omega^*) &= -\frac{4}{\Omega^*}\phi_{\parallel}(\Omega^*),\end{aligned} \tag{14}$$

where the function $\phi_{\parallel}$ was defined by Eq. (9). We introduced the factor, $\hat{\alpha}$, in Eq. (12) which factor is not present (i.e. $\hat{\alpha}=1$, Rüdiger & Kitchatinov 1993) in the mixing-length expression for the alpha-effect by the fluctuating velocities of turbulent convection. It has to be noted here that the nature of the alpha-effect is currently debated. It has been found that not only the fluctuating velocities but also the fluctuating magnetic fields contribute the alpha-effect (Blackman & Field 1999). The new contributions merely reduce the value of α without considerable changes in the structure of the $\boldsymbol{\alpha}$-tensor (Rüdiger et al. 2000). The reduction is accounted by the constant factor $\hat{\alpha}$ in the Eq. (12). The $\hat{\alpha}$-value depends on details of the spectral functions of the turbulent pulsations (Field et al. 1999) which functions are purely known for stellar turbulence. $\hat{\alpha}$ is a free parameter of our model (we actually use the C_α-parameter (28) which is more common for dynamo literature).

Turbulent pumping in inhomogeneous rotating fluids is anisotropic (Kitchatinov 1991),

$$\boldsymbol{\mathcal{E}}_{\rm pump} = \boldsymbol{v}\times\boldsymbol{B} + (\boldsymbol{v}'\times\boldsymbol{e})\,(\boldsymbol{e}\cdot\boldsymbol{B}), \tag{15}$$

so that two effective velocities, $\boldsymbol{v}$ and $\boldsymbol{v}'$, should be specified:

$$\begin{aligned}\boldsymbol{v} &= \eta_{\rm T}\left(\boldsymbol{G}\,\varphi_2(\Omega^*) - \boldsymbol{G}_\perp\varphi_1(\Omega^*)\right),\\ \boldsymbol{v}' &= \eta_{\rm T}\boldsymbol{G}_\perp\left(2\,\varphi_1(\Omega^*) - \varphi_3(\Omega^*)\right),\end{aligned} \tag{16}$$

where $\boldsymbol{G}_\perp=\boldsymbol{G}-\boldsymbol{e}\,(\boldsymbol{e}\cdot\boldsymbol{G})$ is the component of the stratification vector normal to the rotation axis, and further quenching functions are introduced,

$$\begin{aligned}\varphi_3(\Omega^*) &= \frac{3}{8{\Omega^*}^2}\left(1+\frac{2}{1+{\Omega^*}^2}+\frac{{\Omega^*}^2-3}{\Omega^*}\tan^{-1}(\Omega^*)\right),\\ \varphi_1(\Omega^*) &= \phi_{\parallel}(\Omega^*),\ \ \varphi_2(\Omega^*) = \frac{1}{2}\phi(\Omega^*),\end{aligned} \tag{17}$$

where the functions ϕ and $\phi_{\parallel}$ were defined by Eq. (9).

The back reaction of the generated magnetic fields on fluid motion is involved by multiplying the right sides of Eqs. (8), (13), and (16) by the magnetic-quenching functions $\phi_\eta(\beta)$, $\phi_\alpha(\beta)$, and $\phi_v(\beta)$ respectively. The functions depend on the ratio, $\beta = B/B_{\rm eq}$, of magnetic field strength to its energy equipartition value, $B_{\rm eq}=(4\pi\rho\overline{u'^2})^{1/2}$. The functions are specified after the mixing-length expressions derived for the slowly rotating fluids (Rüdiger & Kitchatinov 1993; Kitchatinov et al. 1994),

$$\begin{aligned}\phi_v &= \phi_\eta = \frac{3}{8\beta^2}\left(1+\frac{4+8\beta^2}{(1+\beta^2)^2}+\frac{\beta^2-5}{\beta}\tan^{-1}(\beta)\right),\\ \phi_\alpha &= \frac{15}{32\beta^4}\left(1-\frac{4\beta^2}{3(1+\beta^2)^2}+\frac{\beta^2-1}{\beta}\tan^{-1}(\beta)\right).\end{aligned} \tag{18}$$

The magnetic quenching is of minor importance for dynamo simulations of the present paper because they concern slightly supercritical dynamos for which the field escape through the top boundary is the dominating nonlinearity.

The above formulation relies on a uniform theoretical basis, i.e., it accepts the mean-field expressions for all the basic parameters derived within the same approximations. In this way, it seems possible to avoid multiple free parameters and arbitrary assumptions for which dynamo theories have been repeatedly criticised. Only one free parameter, $\hat{\alpha}$, has been introduced so far.

The convection zone stratification is very close to adiabaticity. The density stratification parameter, $rG=\partial\ln(\rho)/\partial\ln(r)$, for an adiabatically stratified ideal gas with $\gamma=5/3$ is closely reproduced by the expression $rG=-3/2\,(1-x)$, where $x=r/R$ is the fractional radius. This expression diverges, however, on the surface. We replace the stratification parameter by its effective value,

$$rG^* = \frac{rG}{\left(1+\left(\frac{G}{G_0}\right)^n\right)^{\frac{1}{n}}},\ \ rG_0=-20,\ n=3, \tag{19}$$

to keep it finite. The stratification parameter (19) is very close to rG until $rG > rG_0$ and saturates at the value of rG_0 for $rG < rG_0$. Other values of n and rG_0 were tried to confirm that the change of stratification in a thin near-surface layer makes a negligible effect. We put the inner boundary at $x_{\rm i}=0.7$ and prescribe the solar value for the angular velocity, $\Omega_0 = 2.87\cdot 10^{-6}\ {\rm s}^{-1}$.

It remains to specify the equipartition field, $B_{\rm eq}$, the Coriolis number (10), and the eddy diffusivity, $\eta_{\rm T}$. The depth-profiles of the parameters were prescribed after the convection zone model by Stix & Skaley (1990; cf. also Küker et al. 1993) and are shown in Fig. 2.

The absolute majority of the results of this paper belong to the axisymmetric case of the magnetic field independent of the zonal angle ϕ,

$$\boldsymbol{B} = \boldsymbol{e}_\phi B(r,\theta) + {\rm rot}\left(\boldsymbol{e}_\phi\frac{A(r,\theta)}{r\sin\theta}\right). \tag{20}$$

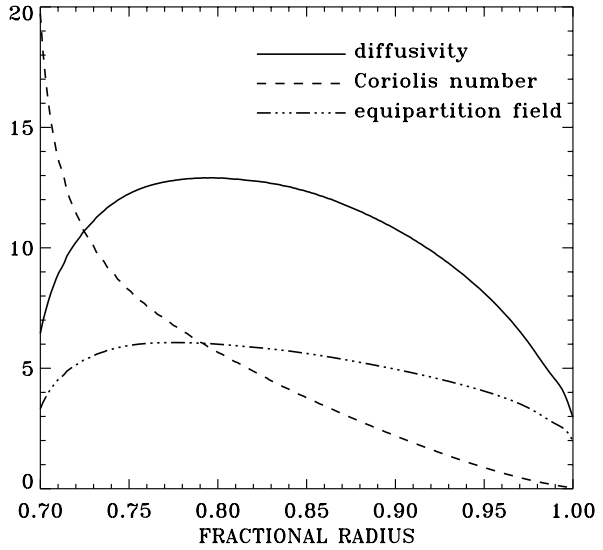

Fig. 2. Eddy diffusivity, $\eta_{\rm T}$, in units of 10^{12} cm^2 s^{-1}; the Coriolis number Ω^* (10); and the equipartition field, $B_{\rm eq}$, in kG as functions of the fractional radius after the solar convection zone model by Stix & Skaley (1990)

In this equation, B is the toroidal field and A is the poloidal field potential. Dynamo equations for the axisymmetric fields are given in the Appendix.

2.2. Boundary conditions

The bottom boundary conditions assume the fluid beneath the convective envelope to be a superconductor and no penetration of magnetic field from the radiative core is allowed,

$$\boldsymbol{n}\times\boldsymbol{\mathcal{E}}=0,\ \ \boldsymbol{n}\cdot\boldsymbol{B}=0,\ \ \text{at } x=x_{\rm i}, \tag{21}$$

where $\boldsymbol{n}$ is the unit vector normal to the boundary.

On the top boundary, we wish to apply a condition different from the usually assumed free escape of magnetic fields. As it has been already noticed in the Introduction, the physical reason for the reduced escape of magnetic flux is the vanishing vertical velocity of convective motions on the top. The vertical turbulent diffusion becomes inefficient there and the field can escape only via the loop eruption instability (Parker 1979). The mean-field approach of the present paper cannot resolve the spatial scales below the correlation length of turbulent motions. Hence, we cannot prescribe a very steep decrease of the vertical diffusivity near the surface and have to formulate the non-free boundary conditions instead.

Consider first the toroidal field. The effective escape velocity, $v_{\rm esc}$, is introduced and the condition for the electromotive force component, $\boldsymbol{\mathcal{E}}_\theta$ (A.3), to fit the escape with a finite rate is imposed,

$$\boldsymbol{\mathcal{E}}_\theta=-v_{\rm esc}B. \tag{22}$$

The escape velocity for the loop eruption instability should be some fraction of the Alfven velocity (Parker 1984). The stability problem for loop eruption has been extensively treated for an atmosphere of an isothermal perfect gas (Parker 1979) which case is far from the partly ionized temperature-stratified stellar subphotospheric plasmas. Nevertheless, we assume that the theory remains qualitatively valid under the stellar conditions so that the escape velocity is proportional to the strength of erupting field (cf. Moss et al. 1999),

$$v_{\rm esc}=\frac{\eta_{\rm T}}{R}\frac{B}{B_0}, \tag{23}$$

where the ratio, $\eta_{\rm T}/R$, of the surface (horizontal) eddy diffusivity to the stellar radius is introduced by dimensional reasons and the field strength, B_0, for which the escape velocity reaches the value of $\eta_{\rm T}/R$ is the second free parameter of our model. The boundary condition (22) now reads

$$\boldsymbol{\mathcal{E}}_\theta+\frac{\eta_{\rm T}}{R}\frac{B^2}{B_0}=0. \tag{24}$$

In the case of very small escape rate, $B\ll B_0$, Eq. (24) reproduces the reflecting boundary condition (21). In the opposite limit of $B_0\to 0$, it reduces to the open boundary condition, $B=0$.

Note that condition (24) does not imply a finite toroidal field *beyond* the top boundary. There may be a surface discontinuity in the radial profile of the field. The correspondent surface current density can exist due to the vanishing vertical diffusivity on the surface (the horizontal scale of the current should be large because the horizontal turbulent mixing does not vanish). A jump in the toroidal field implies, however, a discontinuity in the Maxwell stress,

$$M_{ij}=\left(B_iB_j-\delta_{ij}B^2/2\right)/4\pi. \tag{25}$$

Therefore, a finite surface density of magnetic force may be present with the new boundary condition (24). Though our model does not involve the motion equation, the discontinuity requires the hydrodynamic boundary condition to be considered as well.

Continuity of the angular momentum flux across the surface boundary requires that the cross-component, $T_{r\phi}$, of the total (Reynolds plus magnetic) stress, $T_{ij}=R_{ij}+M_{ij}$, be continuous too. The typical time for establishing MHD equilibrium inside the stellar convection zone ($\sim$10 yr) is much shorter than the characteristic time of variation of the total angular momentum. Accordingly, the appropriate boundary condition for the internal motions can neglect the angular momentum outflow and the stress continuity reduces to the condition of zero surface torque, $T_{r\phi}=0$. The usual vacuum boundary conditions for the magnetic field result in a zero Maxwell stress. Then, the Reynolds stress alone should satisfy the zero torque condition, $R_{r\phi}=0$ (Kippenhahn 1963). The finite toroidal field implied by Eq. (24) requires that the Maxwell stress be restored in the stress-free condition,

$$R_{r\phi}+M_{r\phi}=0\ \ \text{at } r=R. \tag{26}$$

The finite magnetic stress should be balanced by the surface hydrodynamical stress.

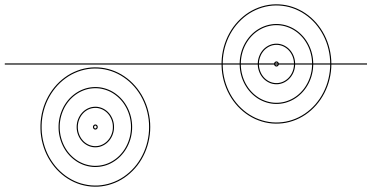

Fig. 3. An illustration of the two basic structures of the poloidal field for which different types of boundary conditions are applied (see the text). The horizontal line signifies the top boundary

Formulating conditions for the poloidal field is much more difficult because its topological properties are quite different from the toroidal field. In spite of no vertical mixing across the top boundary, the poloidal field loops seem to have no difficulties in evolving from the configuration shown in the left of Fig. 3 to that shown in the right. The emergence of the upper part of a loop beyond the top boundary can be easily achieved by a redistribution of the fluid along the field lines. The lines are not actually detached from the fluid over this stage of emergence. An advance of the loop further upward requires an actual detachment of the poloidal field lines and should be prohibited due to zero vertical mixing across the top boundary. The loop in the right of Fig. 3 experiences, however, a diffusive decay due to the horizontal mixing on the top.

Therefore, the condition for the poloidal field should depend on the global field structure. The situation is not at all a new one. The standard vacuum boundary condition for the poloidal field is global as well, for it relates the field state at a given point on the surface to the distribution of the field over the entire surface. We did not find a better possibility than formulating the heuristic conditions that switch from open to closed type depending on the poloidal field configuration. An open-type condition is applied if the field has the topology depicted in the left of Fig. 3. It is changed to a closed-type condition of a slow decay due to the horizontal surface diffusion if the field attains the structure shown in the right of the same figure.

To formulate the condition mathematically, we recall the relation between the poloidal field topology and the distribution of potential A of Eq. (20). Note that A is constant along the field lines and A attains its extremum value in the center of a poloidal field loop. The extremum may be a minimum or a maximum dependent on the sense of circulation of magnetic field vector. The extremum value is equal to the total magnetic flux in the loop per unit azimuthal angle (we fix an arbitrary constant in the definition of A by requiring A to equal zero at the bottom boundary and along the rotation axis).

The field configurations in the left and right of Fig. 3 differ by the radial position, $r_{\max}$, of the extremum of the potential A. It is $r_{\max} < R$ for the left side and $r_{\max} = R$ for the right. We define $r_{\max}$ as the radius of maximum absolute value of A and apply the following boundary condition,

$$\begin{aligned} \frac{\partial A}{\partial r} &= 0 \ \text{ at } r = R \quad \text{if } r_{\max} < R, \\ \frac{\partial A(R)}{\partial t} &= \frac{\eta_{\rm T}(R)}{R^2} \sin\theta \frac{\partial}{\partial\theta} \frac{1}{\sin\theta} \frac{\partial A(R)}{\partial\theta} \quad \text{if } r_{\max} = R. \end{aligned} \tag{27}$$

Table 2. Critical dynamo numbers and oscillation periods for vacuum boundary conditions

Symmetry type	A0	S0	A1	S1
C_α	18.4	18.5	34.9	35.5
$P_{\rm cyc}$(yr)	1.57	1.56	-	-

Eq. $(27)_1$ is the so-called pseudo-vacuum condition. It is applied when $r_{\max} < R$. Starting from the instant when the position $r_{\max}$ arrives on the top, $r_{\max} = R$, the dynamics of the surface potential, $A(R,\theta,t)$, are governed by the diffusion equation $(27)_2$ and the condition for the $A(r,\theta,t)$-function to fit the time-dependent surface profile, $A(R,\theta,t)$, is imposed. The condition switches back to $(27)_1$ when $r_{\max}$ leaves the surface, $r_{\max} < R$.

Eqs. (24) and (27) constitute the boundary conditions by our dynamo model.

3. Results and discussion

We use the standard dimensionless parameter, C_α, to measure efficiency of the alpha-effect,

$$C_\alpha = \frac{\alpha_{\phi\phi} R}{\eta}, \tag{28}$$

where the $\alpha_{\phi\phi}$-component of the $\boldsymbol{\alpha}$-tensor (12) and the diffusivity η are taken at the mid-point, $x = (x_{\rm i}+1)/2$, of the convection zone. Table 2 gives the threshold C_α-values for excitation of magnetic fields of different types of axial and equatorial symmetry found with the traditional vacuum boundary conditions. The capital S and A in the notations of this table stand for the equatorially-symmetric and antisymmetric magnetic fields, respectively, while the number 0 (axisymmetric) or 1 (nonaxisymmetric) signify the azimuthal wave-number.

The nonaxisymmetric modes require much higher dynamo-number for their excitation compared to the axisymmetric ones. The preference for axisymmetry is most probably due to the destructive effect which differential rotation produces on the azimuthally non-uniform fields (Rädler et al. 1990; Rüdiger & Elstner 1994). We do not discuss the nonaxisymmetric modes any further in this paper.

The oscillation periods of Table 2 are much too short to fit the solar activity cycle. Hence, the present model is fully subject to the common defect of solar dynamo models producing activity cycles that are too short when open boundary conditions are applied. It may be also noted that the marginal dynamo with the vacuum boundary conditions is far from the $\alpha\Omega$-regime expected for the Sun. The critical $C_\alpha \simeq 18.4$ given by our $\alpha^2\Omega$-model for this case increases by about 30% when the model is changed to the $\alpha\Omega$-regime.

The reason why the cycles are so short becomes quite evident when the diffusive decay times are estimated. The estimation can be done by switching off all the effects except of turbulent diffusion in the dynamo equation (3). Then, the field dynamics approach eventually the exponential law, $B \sim \exp(-t/\tau)$. For the poloidal and toroidal fields of A0 symmetry type, we find the

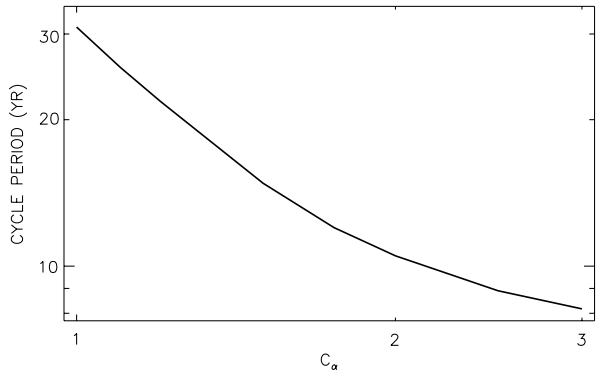

Fig. 4. Cycle period as a function of the dynamo-number C_α (28)

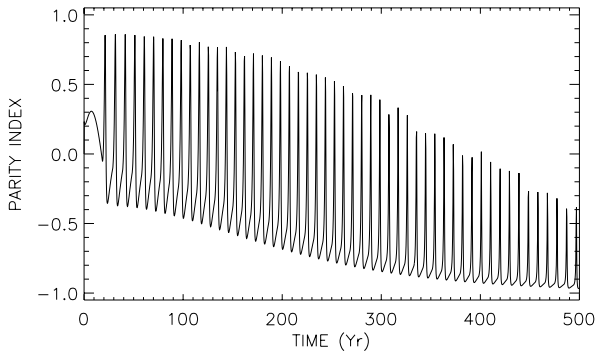

Fig. 5. Time dependence of the equatorial symmetry index (29) for the run started from a state of mixed symmetry. The solution eventually approaches the equatorially-antisymmetric state. $B_0 = 100$ G and $C_\alpha = 1.1$ for this run

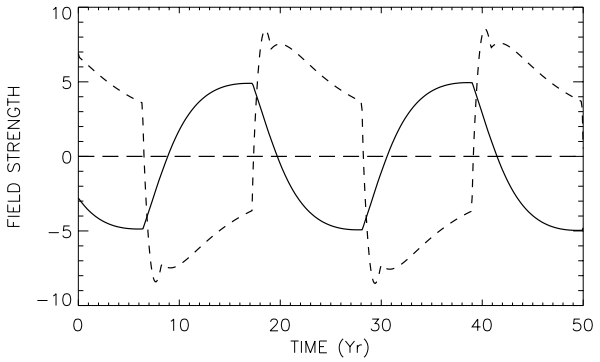

Fig. 6. The surface magnetic field at the pole (dashed) and the toroidal field at a small depth at 45°-latitude (solid). The toroidal field is measured in units of 100 G to present both field components on same plot. The parameters $B_0 = 150$ G and $C_\alpha = 1.2$ of this run provide the best fit for the solar case

decay times $\tau_{\rm pol} = 0.92$ yr and $\tau_{\rm tor} = 0.95$ yr respectively. The oscillation period by dynamo instability cannot exceed considerably the times of decay as discussed in the Introduction.

The decay times increase dramatically when the non-free conditions of the preceding section are applied: $\tau_{\rm tor} = 4.6$ yr and $\tau_{\rm pol} = 26$ yr in this case. The difference between these two values is, probably, due to the horizontal scale of the toroidal component of an equatorially-antisymmetric field is about two times smaller compared to the poloidal field. With the decay times increased so much, we may expect a correspondent increase in the oscillation period and a decrease in the threshold dynamo number.

The dynamo instability insets with quite a low $C_\alpha = 0.98$ with the new boundary conditions. The cycle period of the marginal dynamo mode, $P_{\rm cyc} \simeq 34$ yr, exceeds the solar value. Fig. 4 shows the cycle period of (saturated) nonlinear oscillations as the function of the dynamo number. The plot was obtained with $B_0 = 150$ G in the boundary condition (24). We explain the choice below.

The stable nonlinear solutions show the magnetic field antisymmetric about the equator. The equatorial symmetry can be 'measured' by the parity index (Brandenburg et al. 1989),

$$P = \frac{E^{(S)} - E^{(A)}}{E^{(S)} + E^{(A)}}, \qquad (29)$$

where $E^{(A)}$ and $E^{(S)}$ are the total energies of the antisymmetric and symmetric components of the magnetic field. The runs started from initial states of mixed equatorial symmetry eventually approach the antisymmetric state, $P = -1$. The characteristic example of Fig. 5 shows that the parity relaxation may be quite a long process, however. The preference for equatorially-antisymmetric fields agrees with the observed predominance of dipole-parity component in the global magnetic field of the Sun (Stenflo & Güdel 1988).

Between the two parameters, C_α and B_0, of the present model, C_α mainly controls the cycle period and B_0 defines the generated field amplitude. Judging from the strength of the field emerging in the forming active regions, the toroidal field in the solar convection zone should be about 200–600 G (Lites et al. 1998) during the maximum activity phase. These amplitudes of toroidal field can be reproduced with $B_0 = 150$ G. The cycle period is close to 22 yr with $C_\alpha = 1.2$. Fig. 6 illustrates the run made with these parameter values. Note that the toroidal field is rescaled by the factor of 0.01 on this plot. The $\alpha^2\Omega$ dynamo for open boundary conditions produces toroidal and poloidal fields of comparable strength. Application of the new boundary conditions decreases the poloidal-to-toroidal field ratio by about two orders of magnitude to bring it in closer agreement with observations, though the polar field of Fig. 6 is still larger than $B_{\rm p} \sim 1$–2 G of the Sun. The abrupt changes in the polar field polarity of Fig 6 correspond to the change from the first to second condition in Eq. (27).

Figs. 7 and 8 show the field structure for the basic model reproducing the 22-yr period of the solar activity cycle. The equatorial drift of toroidal field in Fig. 7 cannot be expected from the the rotational law of Fig. 1. The point here is that the guidance provided by the *local* theory of dynamo wave propagation along the isorotational surfaces is not directly applicable to the *global* dynamos. The migration seen in our model is, most probably, due to an emergence of new poloidal flux (cf. the third column of Fig. 8) that leads to the poloidal field amplification on the equatorial side of the emergence region. Then, winding of the

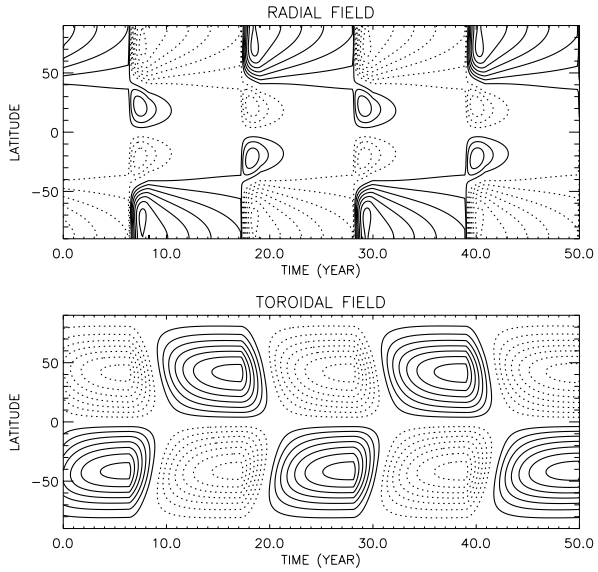

Fig. 7. Butterfly diagram for the case of $C_\alpha = 1.2$, $B_0 = 150$ G showing the cycle period of about 22 yr

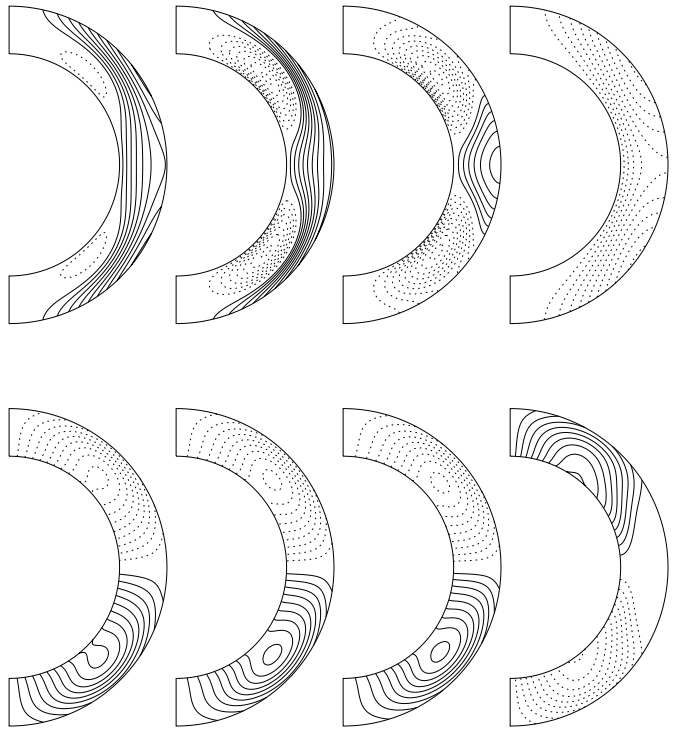

Fig. 8. Poloidal field-lines (top panel) and toroidal field isolines (bottom) for the case of $C_\alpha = 1.2$, $B_0 = 150$ G showing the 22-yr cycle period. Time increases from left to right by the lag of about 3 yr between consecutive columns. Full lines show positive levels and clockwise circulation and v.v. for the dashed lines

poloidal field by differential rotation shifts the maximum of the toroidal field towards the equator.

It has to be noted that the equatorial migration is somewhat too slow and the butterfly 'wings' of Fig. 7 are too broad compared to the Sun. It may be hoped that allowance for meridional flow may change the field migration in the correct way (Roberts & Stix 1972; Dikpati & Charbonneau 1999).

The $P_{\rm cyc}$ versus C_α plot of Fig. 4 is close the relation $P_{\rm cyc} \sim 1/C_\alpha$. For the small C_α represented on this figure, the dynamo operates in the $\alpha\Omega$-regime where only the product, $\mathcal{D} = C_\alpha C_\Omega$, of the two dynamo numbers is relevant ($C_\Omega = \Delta\Omega R^2/\eta$, where $\Delta\Omega$ is the equator-to-pole variation of the angular velocity). Hence, we can write $P_{\rm cyc} \sim 1/\mathcal{D}$. The Coriolis number (10) is well above one even in the slow rotators like the Sun. Eqs. (8) to (13) yield for this case,

$$\mathcal{D} = \frac{\Delta\Omega \alpha_{\phi\phi} R^3}{\eta^2} \sim \Delta\Omega \Omega^{*1.5}, \tag{30}$$

where we took into account that $\eta_{\rm T} \sim \Omega^{*1/2}$ due to the rotational quenching of the thermal eddy diffusivity. The differential rotation model by Kitchatinov & Rüdiger (1999) gives $\Delta\Omega \sim \Omega^{*-p},\ 0 \le p \le 0.5$ for slow rotators. We finally get

$$P_{\rm cyc} \sim (P_{\rm rot}/\tau)^n,\ \ 1 \le n \le 1.5 \tag{31}$$

in close agreement with observational data for slowly rotating stars (Noyes et al. 1984; Saar & Brandenburg 1999). As the rotation rate increases, the dynamo number may eventually exceed the critical value for open boundary conditions violating the relation (31) (Brandenburg et al. 1998).

To sum-up, we note that allowance for a non-free escape of generated magnetic fields from the dynamo region helps to bring the simulated cycle-periods and the poloidal-to-toroidal field ratio in closer agreement with observations.

Acknowledgements. The authors are grateful to the anonymous referee for rising the question on the hydrodynamical boundary conditions. LLK was funded by PPARC grant GR/L00827. This work was supported in part by the Russian Foundation for Basic Research (Project 99-02-16088).

Appendix A: axisymmetric dynamo equations

The mean-field induction equation (3) leads to the following equation for toroidal component of the axisymmetric field (19)

$$\frac{\partial B}{\partial t} = \frac{1}{r}\left(\frac{\partial\Omega}{\partial r}\frac{\partial A}{\partial\theta} - \frac{\partial\Omega}{\partial\theta}\frac{\partial A}{\partial r} + \frac{\partial\,(r\mathcal{E}_\theta)}{\partial r} - \frac{\partial\mathcal{E}_r}{\partial\theta}\right). \tag{A.1}$$

The first two terms on the right side describe the toroidal field production from poloidal field by the differential rotation. The components of mean electromotive force, $\boldsymbol{\mathcal{E}}$ (6), from the right side of the dynamo equation (A.1) read

$$\begin{aligned}
\mathcal{E}_r \ =\ & -\eta_{\rm T}\phi_\eta\bigg(\phi\,\frac{\cos\theta}{r\sin\theta}B + \left(\phi + \phi_{\parallel}\sin^2\theta\right)\frac{1}{r}\frac{\partial B}{\partial\theta} \\
& -\phi_{\parallel}\sin\theta\cos\theta\frac{\partial B}{\partial r}\bigg) \\
& -\ \hat{\alpha}\eta_{\rm T} G\phi_\alpha\bigg(\left(\mathcal{A}_1 + 2\mathcal{A}_2 + \mathcal{A}_4\cos^2\theta\right)\frac{\cos\theta}{r^2\sin\theta}\frac{\partial A}{\partial\theta} \\
& +\left(\mathcal{A}_2 + \mathcal{A}_4\cos^2\theta\right)\frac{1}{r}\frac{\partial A}{\partial r}\bigg) \\
& -\ \eta_{\rm T} G\phi_v\varphi_1\sin\theta\cos\theta\ B,
\end{aligned} \tag{A.2}$$

$$\begin{aligned}\mathcal{E}_\theta &= \eta_{\rm T}\phi_\eta\Bigg(\frac{\phi}{r}\frac{\partial\,(rB)}{\partial r}+\phi_\parallel\cos^2\theta\frac{\partial B}{\partial r}\\ &\quad -\phi_\parallel\sin\theta\cos\theta\frac{1}{r}\frac{\partial B}{\partial\theta}\Bigg)\\ &+\ \hat\alpha\eta_{\rm T}G\phi_\alpha\Bigg(\left(\mathcal{A}_1+\mathcal{A}_4\sin^2\theta\right)\frac{\cos\theta}{r\sin\theta}\frac{\partial A}{\partial r}\\ &\quad +\left(\mathcal{A}_2+\mathcal{A}_4\cos^2\theta\right)\frac{1}{r^2}\frac{\partial A}{\partial\theta}\Bigg)\\ &-\ \eta_{\rm T}G\phi_v\left(\varphi_2-\varphi_1\sin^2\theta\right)B. \end{aligned}\tag{A.3}$$

Dropping the curl in Eq. (3) leads to the following equation for the poloidal field potential,

$$\begin{aligned}\frac{\partial A}{\partial t} &= r\sin\theta\mathcal{E}_\phi\\ &= \eta_{\rm T}\phi_\eta\Bigg(\left(\phi+\phi_\parallel\cos^2\theta\right)\frac{\partial^2 A}{\partial r^2}\\ &\quad +\frac{\phi+\phi_\parallel\sin^2\theta}{r^2}\sin\theta\frac{\partial}{\partial\theta}\frac{1}{\sin\theta}\frac{\partial A}{\partial\theta}+\frac{\phi_\parallel}{r}\sin^2\theta\frac{\partial A}{\partial r}\\ &\quad +\frac{3\phi_\parallel}{r^2}\sin\theta\cos\theta\frac{\partial A}{\partial\theta}-\frac{2\phi_\parallel}{r}\sin\theta\cos\theta\frac{\partial^2 A}{\partial r\partial\theta}\Bigg)\\ &+\ \eta_{\rm T}G\phi_v\Bigg(\left((\varphi_3-\varphi_1)\sin^2\theta-\varphi_2\right)\frac{\partial A}{\partial r}\\ &\quad +(\varphi_3-\varphi_1)\sin\theta\cos\theta\frac{1}{r}\frac{\partial A}{\partial\theta}\Bigg)\\ &-\ \hat\alpha\eta_{\rm T}G\phi_\alpha\mathcal{A}_1 r\sin\theta\cos\theta B. \end{aligned}\tag{A.4}$$

Note that all three components, (A.2), (A.3), and (A.4), of the mean electromotive force scale with the eddy diffusivity, $\eta_{\rm T}$. It means that an increase of the diffusivity by a constant factor leads to a decrease of the dynamo-cycle period in about the same proportion.

References

Alekseev I.Yu., Gershberg R.E., 1998, A probable periodicity in the activity of the red dwarf flare star EV Lac. In: Donahue R.A., Bookbinder J.A. (eds.) The Thenth Cambridge Workshop on Cool Stars, Stellar Systems and the Sun. PASPC 154, 1471

Baliunas S., Donahue R.A., Soon W.H., et al., 1995, ApJ 438, 269

Belvedere G.M., Kuzanyan K.M., Sokoloff D., 2000, MNRAS (submitted)

Blackman E.G., Field G.B., 1999, ApJ 521, 597

Brandenburg A., Krause F., Meinel R., Moss D., Tuominen I., 1989, A&A 213, 411

Brandenburg A., Saar S.H., Turpin C.R., 1998, ApJ 498, L51

Chandrasekhar S., 1961, Hydrodynamic and hydromagnetic stability. Clarendon Press, Oxford

Dikpati M., Charbonneau P., 1999, ApJ 518, 508

Donati J.-F., 1999, MNRAS 302, 457

Donati J.-F., Cameron A.C., 1997, MNRAS 291, 1

Donati J.-F., Cameron A.C., Hussain G.A.J., Semel M., 1999, MNRAS 302, 457

Field G.B., Blackman E.G., Chou H., 1999, ApJ 513, 638

Kippenhahn R., 1963, ApJ 137, 664

Kippenhahn R., Weigert A., 1994, Stellar Structure and Evolution. Springer, Berlin

Kitchatinov L.L., 1991, A&A 243, 483

Kitchatinov L.L., Pipin V.V., 1993, A&A 274, 647

Kitchatinov L.L., Rüdiger G., 1999, A&A 344, 911

Kitchatinov L.L., Pipin V.V., Rüdiger G., 1994, Astron. Nachr. 315, 157

Kosovichev A.G., Schou J., Scherrer P.H., et al., 1997, Solar Phys. 170, 43

Krause F., Rädler K.-H., 1980, Mean–Field Magnetohydrodynamics and Dynamo Theory. Akademieverlag, Berlin

Küker M., Rüdiger G., Kitchatinov L.L., 1993, A&A 279, L1

Lites B.W., Skumanich A., Martinez Pillet V., 1998, A&A 333, 1053

Moss D., Shukurov A.M., Sokoloff D.D., 1999, A&A 343, 120

Nordlund A., Brandenburg A., Jennings R.L., et al., 1992, ApJ 392, 647

Noyes R.W., Weiss N.O., Vaughan A.H., 1984, ApJ 287, 769

Parker E.N., 1979, Cosmic magnetic fields, Clarendon press, Oxford

Parker E.N., 1984, ApJ 281, 839

Rädler K.-H., Wiedemann E., Meinel R., Brandenburg A., Tuominen I., 1990, A&A 239, 413

Roberts P.H., Stix M., 1972, A&A 18, 453

Rüdiger G., 1989, Differential rotation and stellar convection: sun and solar-type stars. Gordon & Breach, New York

Rüdiger G., 1994, Dynamo theory and the period of the solar cycle. In: Solar Magnetic Fields, eds. Schüssler M., Schmidt W., Cambridge Univ. Press, p. 77

Rüdiger G., Elstner D., 1994, A&A 281, 46

Rüdiger G., Kitchatinov L.L., 1993, A&A 269, 581

Rüdiger G., Pipin V.V., Belvedere G., 2000, Solar Phys. (submitted)

Saar S.H., Brandenburg A., 1999, ApJ 524, 295

Stenflo J.O., Güdel M., 1988, A&A, 191, 137

Stix M., 1995, Solar models with convective overshoot. In: Workshop on Solar Modelling, eds. Bahcall J.N., Balantekin B., World Scientific, p. 199

Stix M., Skaley D., 1990, A&A 232, 234

Tuominen I., Brandenburg A., Moss D., Rieutord M., 1994, A&A 284, 259